

LARGER ABSOLUTE BAND GAPS IN TWO-DIMENSIONAL PHOTONIC CRYSTALS FABRICATED BY A THREE-ORDER-EFFECT METHOD

H. Li and X. Yang

MOE Key Laboratory of Laser Life Science
and Institute of Laser Life Science
South China Normal University
Guangzhou 510631, China

Abstract—In this paper, based on different influences of the lattice symmetry, the geometry of dielectric rod, and the structure of unit cell to absolute gaps we propose a so-called three-order-effect method for the construction of two-dimensional (2D) photonic crystals (PCs) with larger absolute gaps. As an example, by means of our approach we fabricate a 2D hexagonal lattice of cylinder with an optimal rod adding at the center of the unit cell, where the absolute gap is larger than that of the PC with similar structure studied by other group previously. On the other hand, we also find that many of the 2D PCs with larger absolute gaps reported previously possess optimal first-order and second-order substructures. Our three-order-effect method would be useful for the design of 2D PCs with larger absolute gaps.

1. INTRODUCTION

Periodic dielectric structures on a wavelength scale exhibit photonic band gaps (PBGs) [1, 2], where the propagating modes of electromagnetic (EM) wave are forbidden. Being a kind of important PBG structures, photonic crystals (PCs) have been investigated theoretically and experimentally [3–9].

Many significant applications of PCs are based on the absolute photonic band gaps [10–13], and the larger the width of the absolute band gap is, the better the characteristic will be. Previous studies show that the absolute gaps in a two-dimensional (2D) lattice can be

obviously increased by reducing the total symmetry of a PC [14–16], but in order to obtain larger absolute gaps for a given PC, how to reduce the structure symmetry and what extent the symmetry can be reduced to are still uncertain.

In this paper, we study the absolute gaps of 2D PCs with different geometry structures and find that the lattice symmetry has a decisive effect on the widths of absolute gaps, that the geometry of dielectric rod plays an important role in the controlling of the widths of absolute gaps, and that the structure of a unit cell can influence the widths of absolute gaps to a significant degree. Based on these results we propose a so-called three-order-effect method for the construction of 2D PCs with larger absolute gaps and point out that a hexagonal lattice and a cylindric dielectric rod are the optimal first-order and second-order substructures, respectively. Although the general optimal third-order substructure cannot be determined simply, here we provide an effective approach to seek the optimal third-order substructure. Inserting optimal rods and/or connecting slabs at the points/sides, which correspond to the places with high symmetry of the first Brillouin zone, one can change the shapes and/or positions of photonic bands and decrease the degree of degeneracy of the bands, and then wider absolute gaps may be created. As an example, by means of our approach we fabricate a 2D hexagonal lattice of cylinder with an optimal rod adding at the center of the unit cell. It is found that the absolute gap created by this PC is larger than that of the PC with similar structure studied by other group previously [10]. On the other hand, one can see that the first-order and second-order substructures of the 2D PCs with wider absolute gaps reported formerly are all optimal [10, 13]. Further, we compare our three-order-effect method with other corresponding approaches and find that the structures constructed by our method are better than those reported previously. The three-order-effect technique would provide a new method for the designing of 2D PCs with wider absolute gaps.

This paper is organized as follows. In Section 2, we introduce the theory for calculating band structures of 2D PCs. The three-order-effect method is presented in Section 3. In Section 4, we give the results and discussions. Finally the conclusions are drawn in Section 5.

2. THEORY

For linear isotropic and frequency-independent dielectric materials with permeability close to 1.0, the time-harmonic modes in two

dimensions for E polarization can be expressed as

$$\frac{1}{\varepsilon(\bar{r})} \left\{ \frac{\partial^2}{\partial x^2} + \frac{\partial^2}{\partial y^2} \right\} E(\bar{r}, t) = \frac{1}{c^2} \frac{\partial^2}{\partial t^2} E(\bar{r}, t), \quad (1)$$

and H polarization as

$$\left\{ \frac{\partial}{\partial x} \frac{1}{\varepsilon(\bar{r})} \frac{\partial}{\partial x} + \frac{\partial}{\partial y} \frac{1}{\varepsilon(\bar{r})} \frac{\partial}{\partial y} \right\} H(\bar{r}, t) = \frac{1}{c^2} \frac{\partial^2}{\partial t^2} H(\bar{r}, t), \quad (2)$$

where $E(\bar{r}, t)$ and $H(\bar{r}, t)$ are the electric and magnetic field intensities, respectively, and $\varepsilon = \varepsilon(\bar{r})$ is the dielectric function. The periodicity of $\varepsilon(\bar{r})$ implies

$$\varepsilon(\bar{r} + \bar{a}_j) = \varepsilon(\bar{r}), \quad (j = 1, 2), \quad (3)$$

where \bar{a}_j is the elementary lattice vector of the 2D PC. Being spatial periodic $1/\varepsilon(\bar{r})$ can be expanded in the following Fourier series:

$$\frac{1}{\varepsilon(\bar{r})} = \sum_{\bar{G}} k(\bar{G}) \exp(i\bar{G} \cdot \bar{r}), \quad (4)$$

where \bar{G} is the reciprocal vector. By use of Bloch's theorem $E(\bar{r})$ and $H(\bar{r})$ can be expressed as

$$E(\bar{r}) = E_{kn}(\bar{r}) = \sum_{\bar{G}} E_{kn}(\bar{G}) \exp\{i(\bar{k} + \bar{G}) \cdot \bar{r}\} \quad (5)$$

and

$$H(\bar{r}) = H_{kn}(\bar{r}) = \sum_{\bar{G}} H_{kn}(\bar{G}) \exp\{i(\bar{k} + \bar{G}) \cdot \bar{r}\}, \quad (6)$$

where \vec{k} is a 2D wave vector and n is a band index. Substituting Eqs. (5) ((6)) into Eqs. (1) ((2)) one can obtain the following eigenvalue equations for the expansion coefficients:

$$\sum_{\bar{G}'} k(\bar{G} - \bar{G}') \left| \bar{k} + \bar{G}' \right|^2 E_{kn}(\bar{G}') = \frac{\omega_{kn}^2}{c^2} E_{kn}(\bar{G}) \quad (7)$$

and

$$\sum_{\bar{G}'} k(\bar{G} - \bar{G}') (\bar{k} + \bar{G}') \cdot (\bar{k} + \bar{G}') H_{kn}(\bar{G}') = \frac{\omega_{kn}^2}{c^2} H_{kn}(\bar{G}). \quad (8)$$

Then one can calculate photonic bands by solving Eqs. (7) and (8). In this paper, we focus on investigating the relationship between lattice structures and absolute gaps and have not paid much attention to the the convergence of the calculation. All of our simulations are obtained by means of "BandSOLVE 1.3" of "Rsoft" software, where the grid is chosen to be 128×128 .

3. THREE-ORDER-EFFECT METHOD

For the different influences to the absolute gaps, we separate a 2D PC into three orders of substructures and propose a so-called three-order-effect method for the construction of 2D PCs with larger absolute gaps.

3.1. Optimal First-order Substructure

In Fig. 1, we show three kinds of simple lattices of regular quadrangular prism and calculate the widths of the absolute gaps of these 2D PCs, respectively. The relationship between the gap-midgap ratio and the filling fraction is plotted in Fig. 2.

From Fig. 2, one can see that (1) for the triangular lattice the absolute band gaps appear at the filling fractions of 0.26–0.33, 0.40–0.53, and 0.59–0.63, respectively, and the largest absolute gap-midgap ratio is 0.023986; (2) for the square lattice the band gap appears at the filling fraction of 0.20–0.48 and the absolute gap-midgap ratio is

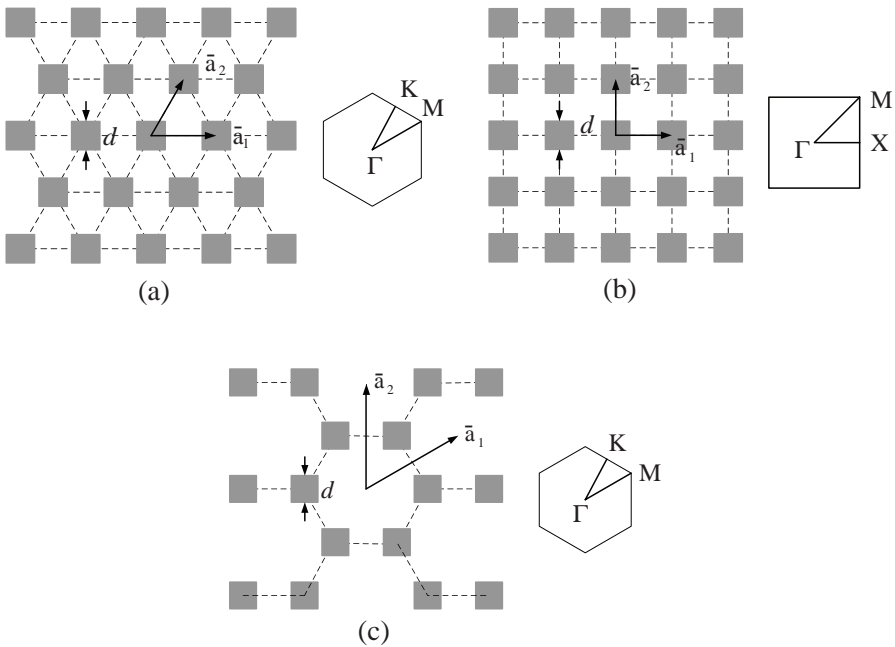


Figure 1. Three kinds of lattices of regular quadrangular prism and their first Brillouin zones, where \bar{a}_1 and \bar{a}_2 are the translation vectors and d is the side length of a regular quadrangular prism. (a) Triangular lattice. (b) Square lattice. (c) Hexagonal lattice.

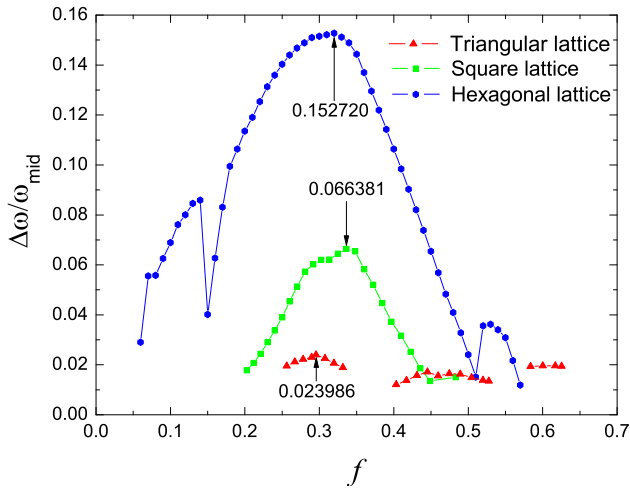


Figure 2. The relationship between gap-midgap ratio and filling fraction for the lattices shown in Fig. 1, where the dielectric contrast is $\varepsilon/\varepsilon_0 = 16$.

less than 0.066381; (3) for the hexagonal lattice the band gap appears at the filling fraction of 0.06–0.57 and the absolute gap-midgap ratio is less than 0.152720. The average absolute gap-midgap ratio of the hexagonal lattice is much larger than that of the square lattice and that of the triangular lattice is very small. It means that for the same dielectric contrast and same kinds of prisms, the hexagonal lattice can create largest absolute gap.

Obviously, the lattice symmetry influences decisively the positions and widths of absolute gaps and the effect of the lattice symmetry for creating absolute gaps is the first order effect. So, we call the basic lattice structure the first-order substructure. For 2D PCs there are only three kinds of basic lattice structures, the triangular, square and hexagonal lattices. Based on the results shown in Fig. 2 our three-order-effect method points out that the hexagonal lattice shown in Fig. 1(c) is the optimal first-order substructure.

On the other hand, the plane group symmetries of the triangular, square and hexagonal lattices are 6 mm, 4 mm, and 3 m, respectively. From the point of view of the lattice symmetry, the reduction of symmetry can significantly increase the size of absolute gaps [10]. Our three-order-effect method points out that in order to obtain larger absolute gaps the symmetry of the first-order substructure should be reduced to the minimum.

3.2. Optimal Second-order Substructure

Based on the optimal first-order substructure, we now investigate the influence of the rod shape on absolute gaps. The results for the relationship between the largest absolute gap-midgap ratio and the rod shape are shown in Table 1.

From Table 1, one can see that the maximal absolute gap-midgap ratio increases monotonously with the increment of the side number of cross sections of rods and the maximal absolute gap-midgap ratio of the hexagonal lattice of cylinder is 1.555 times larger than that of triangular prism. On the other hand, when the side number of the cross section of a rod is bigger than 5, the filling fraction of the maximal absolute gap-midgap ratio keeps approximately constant. It means that the rod shape plays an important role in the controlling of the width of absolute gaps and the effect of the rod shape for creating absolute gaps is the second order effect. So, we call the shape of the rod at the lattice point, but not in the unit cell, the second-order substructure. Based on the results shown in Table 1, our three-order-effect method points out that cylinder is the optimal second-order substructure.

Table 1. The data of the maximal absolute gaps of the hexagonal lattices of eleven kinds of rods, where the 1st column shows the shapes of cross sections of rods, the 2nd column gives the filling fractions of the lattice for the maximal absolute gaps, the 3rd column provides the widths of the maximal absolute gaps, the 4th column lists the mid-frequencies of the maximal absolute gaps, and the 5th column writes out the maximal absolute gap-midgap ratios. The dielectric contrast is $\varepsilon/\varepsilon_0 = 16$ and a is the lattice constant.

Cross section of Rod	f	$a\Delta\omega/2\pi c$	$a\omega_{\text{mid}}/2\pi c$	$\Delta\omega/\omega_{\text{mid}}$
Regular Triangle	0.350	0.032737	0.323365	0.101238
Square	0.320	0.051138	0.334850	0.152720
Regular Pentagon	0.295	0.053169	0.342398	0.155285
Regular Hexagon	0.295	0.053400	0.342000	0.155891
Regular Heptagon	0.295	0.053505	0.341852	0.156516
Regular Octagon	0.295	0.053600	0.342000	0.156691
Regular Nonagon	0.295	0.053600	0.342000	0.156746
Regular Decagon	0.295	0.053546	0.341544	0.156776
Regular Dodecagon	0.295	0.053692	0.341608	0.157174
Regular Hexadecagon	0.295	0.053722	0.341592	0.157268
Circle	0.295	0.053775	0.341590	0.157427

3.3. Third-order Substructure

For many 2D PCs there exist band gaps of some polarizations, but these gaps may not overlap to generate absolute ones or the size of absolute band gaps is often limited by band degeneracies at the lattice symmetry points [14, 16]. By reducing the the symmetry of the unit cell, these degeneracies can be lifted and wider absolute gaps can be obtained, for the 2D more symmetric PCs new absolute gaps can be created [14]. The reduction of the symmetry of the unit cell can be achieved by inserting dielectric geometrical structures at well-chosen place(s). That is to say, absolute gaps can be widened by changing the symmetry of the unit cell and the structure of a unit cell can influence the widths of absolute gaps to a significant degree. For generating absolute gaps the effect of the structure of a unit cell is the third order effect and we call the structure of a unit cell the third-order substructure.

Not as determinable as the first-order and second-order substructures, the general optimal third-order substructure can not be determined simply. Based on the aforementioned principle of the reduction of the symmetry of a unit cell, our three-order-effect method suggests an effective approach to seek the optimal third-order substructures as follows. In the unit cell of a hexagonal lattice of cylinder, one can obtain the optimal third-order substructures by inserting optimal rods and/or connecting slabs at the symmetric points/sides. Here, we keep the optimal first-order and second-order substructures, but not the filling fractions, unchanged.

For example, we compare the result of the square lattice reported in [14] with that obtained by our three-order-effect method. The square lattice is illustrated in Fig. 3. In [14], the filling fraction keeps to be 0.33, and the maximal absolute gap-midgap ratio was searched by scanning radius ratio $\beta = r_2/r_1$. It was found that the maximal absolute gap-midgap ratio $\Delta\omega/\omega_{\text{mid}} = 0.037234$ occurs at $\beta = 0.57$. In our calculation, the radius of the bigger rod r_1 keeps to be $0.3241a$, where a is the lattice constant, and the maximal absolute gap-midgap ratio is searched by scanning the radius of the smaller rod r_2 . The maximal absolute gap-midgap ratio we obtained is $\Delta\omega/\omega_{\text{mid}} = 0.038989$ at $\beta = 0.615$ (see Fig. 4). One can see that our result is 4.71% larger than that reported in [14].

On the other hand, Sigmund and Hougaard [17] recently proposed an interesting approach for the optimization of PC structures. By means of this method larger TM and TE gaps can be created by the elliptic rods with centers defined by the generators of an optimal centroidal Voronoi tessellation and the walls of this tessellation. Although systematic results can not be obtained when

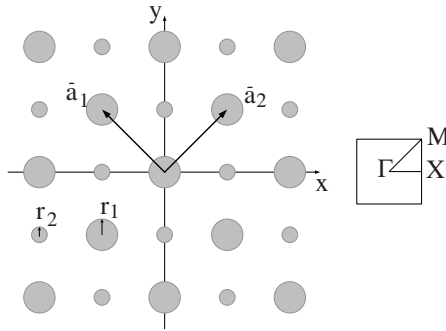


Figure 3. The square lattice with two kinds of rods and its first Brillouin zone, where \bar{a}_1 and \bar{a}_2 are the translation vectors ($\bar{a}_1 = -\frac{\sqrt{2}}{2}a\bar{e}_x + \frac{\sqrt{2}}{2}a\bar{e}_y$, $\bar{a}_2 = \frac{\sqrt{2}}{2}a\bar{e}_x + \frac{\sqrt{2}}{2}a\bar{e}_y$) and r_1 and r_2 are the radii of the bigger and smaller rods, respectively.

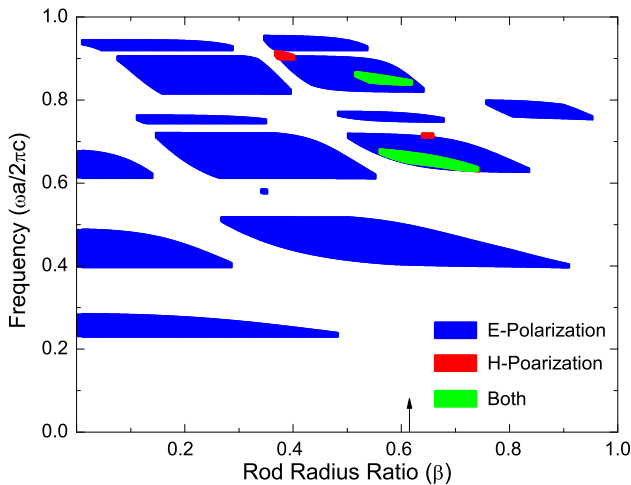


Figure 4. Gap map for the square lattice shown in Fig. 3, where the radius of the bigger rod is $r_1 = a\sqrt{f/\pi} = a\sqrt{0.33/\pi} = 0.3241a$ and the dielectric contrast is $\epsilon/\epsilon_0 = 11.4$. The maximal absolute gap occurs at $\beta = 0.615$ (arrow).

this optimization algorithm is applied to the case of full gaps, Ref. [17] provided a new understanding of the problem of PC structure optimization. Our three-order-effect method may not be effective for the designing of the 2D PCs with larger TM or TE gaps, but will be useful for the construction of the 2D PCs with larger simultaneous TM

and TE gaps, because the optimal first-order substructure, a hexagonal lattice and the second-order substructure, a cylindric dielectric rod would be a major contribution towards the generation of larger absolute gaps, and inserting optimal rods and/or connecting slabs at the symmetry points/sides of the unit cell can change the shapes and/or positions of photonic bands and then enlarge the overlap degree of TM and TE gaps significantly.

4. RESULTS AND DISCUSSIONS

In order to demonstrate the effective methods of seeking optimal third-order substructures, in this section we show two kinds of optimizational 2D PCs and analyse the influence of the third-order substructure to the absolute gaps.

4.1. Hexagonal Lattice of Cylinder with Connecting Slabs

Reference [13] reported an effective structure with larger absolute gaps, where the connecting slabs are inserted on the boundary of each unit cell (see Fig. 5). The design principle of this PC is accordant with that of our three-order-effect method. In this subsection, we analyse the influence of the three-order substructure to absolute gaps. For simplicity, here we call the crystal shown in Fig. 5 the complex lattice and the hexagonal lattice of cylinder without connecting slabs the simple one, respectively.

Figures 6(a) and 6(b) show the band structures of *E*-polarization of the simple and complex lattices in the range of $0 \sim 0.8(\omega a/2\pi c)$,

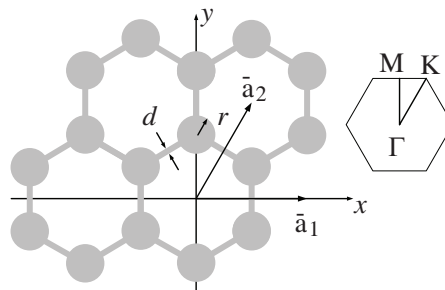


Figure 5. The hexagonal lattice of cylinder with connecting slabs and its first Brillouin zone, where \bar{a}_1 and \bar{a}_2 are translation vectors ($\bar{a}_1 = a\bar{e}_x$, $\bar{a}_2 = \frac{1}{2}a\bar{e}_x + \frac{\sqrt{3}}{2}a\bar{e}_y$) and r and d are the radius of a cylinder and the width of a connecting slab, respectively.

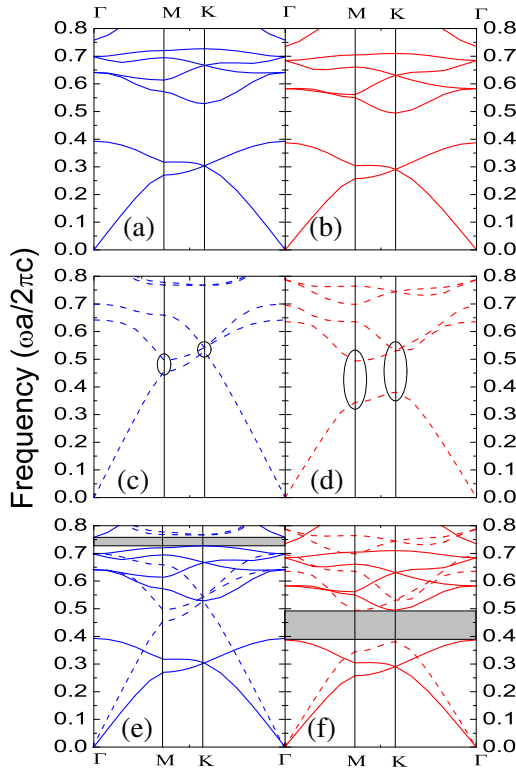


Figure 6. The band structures for the simple lattice with $r = 0.155a$ and the complex lattice shown in Fig. 5 with $r = 0.155a$ and $d = 0.035a$. (a) and (b) are the TE spectra for the simple and complex lattices, respectively. (c) and (d) are the TM spectra for the simple and complex lattices, respectively. (e) and (f) are the TE and TM spectra for the simple and complex lattices, respectively.

respectively, where there exist two band gaps. The corresponding mid-frequencies in Fig. 6(a) are $\omega_{\text{mid1}}^{(E)} = 0.460526(\omega a/2\pi c)$ and $\omega_{\text{mid2}}^{(E)} = 0.742506(\omega a/2\pi c)$, respectively. Those in Fig. 6(b) are $\omega_{\text{mid1}}^{\prime(E)} = 0.440836(\omega a/2\pi c)$ and $\omega_{\text{mid2}}^{\prime(E)} = 0.722563(\omega a/2\pi c)$, respectively. These two band structures are very similar to each other while the latter is lower than that of the former. It means that the three-order substructure of the connecting slabs makes the two TE gaps lower.

Figures 6(c) and 6(d) show the band structures of H -polarization of the simple and complex lattices in the range of $0 \sim 0.8(\omega a/2\pi c)$, respectively, where there exists only one small band gap. In Fig. 6(c),

$\omega_{\text{mid}}^{(H)} = 0.733270(\omega a/2\pi c)$. From Fig. 6(d), one can see that after inserting slabs on the boundary of each unit cell, the first band of the complex lattice at points M and K moves lower, this results in a larger TM gap in the range of $0.380959 \sim 0.493575(\omega a/2\pi c)$ and its $\omega_{\text{mid}}^{(H)} = 0.437267(\omega a/2\pi c)$. It means that the three-order substructure of the connecting slabs makes the TM gap not only wider but also closer to the corresponding TE gap.

Figures 6(e) and 6(f) show the absolute band structures of the simple and complex lattices in the range of $0 \sim 0.8(\omega a/2\pi c)$, respectively. Comparing with Figs. 6(e) and 6(f) one can see that the first band gaps of *E*- and *H*-polarizations of the complex lattice overlap much more sufficiently than those of the simple lattice, this makes the width of the absolute gap of the complex lattice be 30% larger than that of the simple lattice [13]. It shows that inserting appropriate slabs on the boundary of each unit cell is one of the effective methods to search an optimal third-order substructure.

4.2. Hexagonal Lattice of Cylinder with Inserting Cylinders

By means of our three-order-effect approach we design another kind of effective structure for the generating of larger absolute gaps, where the optimal cylinder is inserted at the the center of each unit cell (see Fig. 7). For simplicity, in this subsection we call the crystal shown in Fig. 7 the complex lattice and that without inserting rods the simple one.

Figures 8(a) and 8(b) show the band structures of *E*-polarization

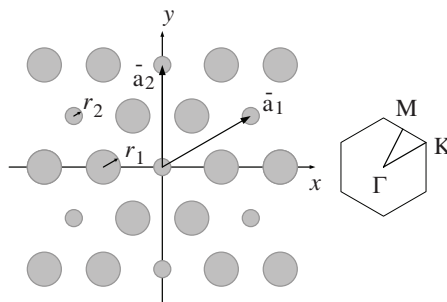


Figure 7. The hexagonal lattice of cylinder with inserting rods and its first Brillouin zone, where \bar{a}_1 and \bar{a}_2 are translation vectors ($\bar{a}_1 = \frac{\sqrt{3}}{2} a \bar{e}_x + \frac{1}{2} a \bar{e}_y$, $\bar{a}_2 = a \bar{e}_y$) and r_1 and r_2 are the radii of the bigger and smaller cylinders, respectively.

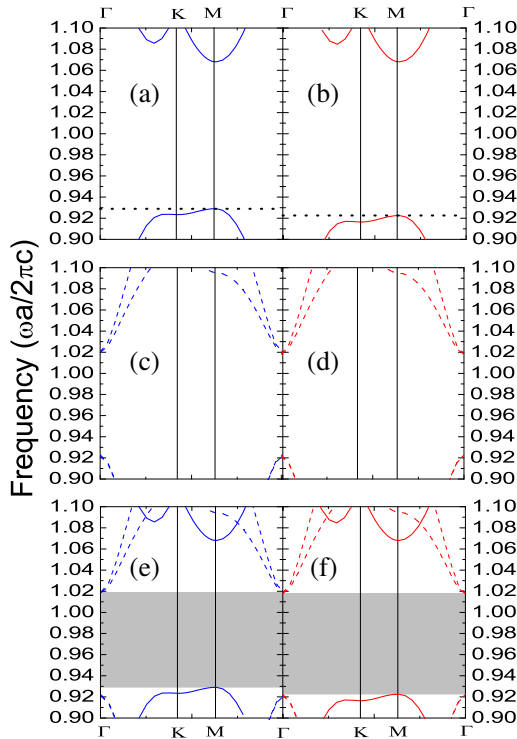


Figure 8. The band structures for the simple lattice with $r_1 = 0.1389a$ and the complex lattice shown in Fig. 7 with $r_1 = 0.1389a$ and $r_2 = 0.082r_1$. (a) and (b) are the TE spectra for the simple and complex lattices, respectively. (c) and (d) are the TM spectra for the simple and complex lattices, respectively. (e) and (f) are the TE and TM spectra for the simple and complex lattices, respectively.

of the simple and complex lattices in the range of $0.9 \sim 1.1(\omega a/2\pi c)$, respectively, where there exists one band gap. The ranges of the band gaps in Figs. 8(a) and 8(b) are $0.929091 \sim 1.067988(\omega a/2\pi c)$ and $0.922563 \sim 1.067994(\omega a/2\pi c)$, respectively. The corresponding mid-frequencies in Figs. 8(a) and 8(b) are $\omega_{\text{mid}}^{(E)} = 0.998539(\omega a/2\pi c)$ and $\omega_{\text{mid}}^{(E)} = 0.995279(\omega a/2\pi c)$, respectively. Obviously, the three-order substructure of the inserting rod makes the TE gap wider and lower. Here the dashed lines denote the lower boundary of the band gap.

Figures 8(c) and 8(d) show the band structures of H -polarization of the simple and complex lattices in the range of $0.9 \sim 1.1(\omega a/2\pi c)$, respectively, where there exists one band gap. The ranges of the band

gaps in Figs. 8(c) and 8(d) are $0.922965 \sim 1.019795(\omega a/2\pi c)$ and $0.922632 \sim 1.018037(\omega a/2\pi c)$, respectively. The corresponding mid-frequencies in Figs. 8(c) and 8(d) are $\omega_{\text{mid}}^{(H)} = 0.971380(\omega a/2\pi c)$ and $\omega_{\text{mid}}^{(H')} = 0.970335(\omega a/2\pi c)$, respectively. It means that the three-order substructure of the inserting rods makes the TM gap slightly wider and lower.

Figures 8(e) and 8(f) show the absolute band structures of the simple and complex lattices in the range of $0.9 \sim 1.1(\omega a/2\pi c)$, respectively. Comparing with Figs. 8(e) and 8(f) one can see that the band gaps of *E*- and *H*-polarizations of the complex lattice overlap more sufficiently than that of the simple lattice, this makes the width of the absolute gap of the complex lattice be larger than that of the simple lattice. Fig. 9 shows the gap map for the hexagonal lattice of cylinder shown in Fig. 7 as a function of the cylinder radius ratio, β ($\beta = r_2/r_1$). One can see that the maximal absolute gap occurs at $\beta = 0.082$ and the maximal gap-midgap ratio is 0.098322. It shows that inserting an appropriate rod at the center of each unit cell is also one of the effective methods to search an optimal third-order substructure.

We emphasize that the structure shown in Fig. 7 is similar to that reported in [10], but our construction method is different from

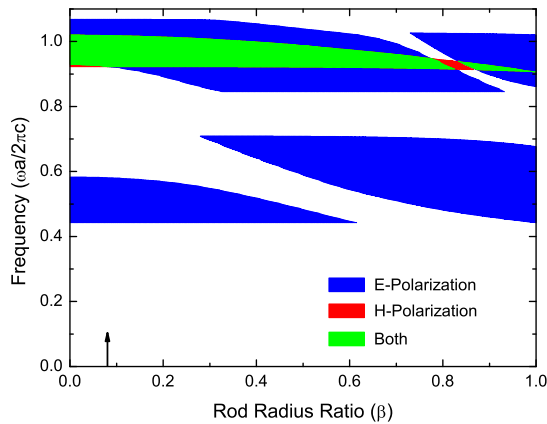


Figure 9. Gap map for the hexagonal lattice of cylinder shown in Fig. 7 as a function of the cylinder radius ratio, β , where $r_1/a = \sqrt{\frac{\sqrt{3}}{4\pi} f} = \sqrt{\frac{\sqrt{3}}{4\pi}} \times 0.14 = 0.1389$ and the dielectric contrast is $\epsilon/\epsilon_0 = 11.4$. The maximal absolute gap occurs at $\beta = 0.082$ (arrow).

theirs. In [10], the filling fraction was kept invariable and the optimal structure was searched by scanning the radius ratio β . We keep the lattice type and rod radius r_1 unaltered, where r_1 is the optimal radius of the maximal absolute gaps of the hexagonal lattice of cylinder, and then search the optimal third-order substructure by scanning β . The absolute gap-midgap ratio of our structure is 0.03% larger than that reported in [10].

In a word, for our three-order-effect method the first-order and second-order substructures should be kept unchanged during the construction of the 2D PC with larger absolute gaps, i.e., the optimal PC structure can be simply obtained by seeking the optimal third-order substructure of the hexagonal lattice of cylinder. So constructing a clever unit cell structure is the effective approach for the designing of 2D PCs with larger absolute gaps.

5. CONCLUSION

In this paper, we make use of the plane-wave expansion method to calculate the band spectra of 2D PCs with different geometry structures and propose the three-order-effect method to construct 2D PCs with larger absolute gaps.

Firstly, the widths of absolute gaps of quadrangular prisms arrayed in three kinds of simple lattices have been calculated, and it is found that the average absolute gap-midgap ratio of the hexagonal lattice is much larger than that of the square lattice and that the average absolute gap-midgap ratio of the square lattice is also much larger than that of the triangular lattice. It means that for the same dielectric contrast and same kind of prisms, only the hexagonal lattice can yield the largest absolute gap. The lattice symmetry influences the generation and width of absolute gaps decisively, and we call the lattice structure the first-order substructure. For 2D PCs, a hexagonal lattice is the optimal first-order substructure.

Secondly, the influence of rod shapes has been also considered. It is found that the maximal absolute gap-midgap ratio of cylinders arrayed in hexagonal lattice is 1.555 larger than that of regular triangular prisms and that a cylinder is the best substructure among all the prisms. So the rod shape plays an important role in controlling the width of absolute gaps, and we call the geometric structure of rod the second-order substructure. For 2D PCs, a cylinder is the optimal second-order substructure.

Thirdly, the third-order substructure is much more complicated than the first-order and second-order ones. Analyzing the relationship between the widths of band gaps and the structures of unit cells, one

knows that absolute gaps can be widened by changing the symmetry of each unit cell and that the structure of a unit cell can influence absolute gaps to a significant degree. So, we define the structure of a unit cell as the third-order substructure. By the use of our three-order-effect method we fabricate two kinds of 2D PCs with larger absolute gaps by inserting appropriate rods and/or connecting slabs in each unit cell while the first-order and second-order substructures keep unchanged. The widths of absolute gaps for our constructed 2D PCs are larger than those of the similar structures reported previously.

On the other hand, it is also found that the first-order and second-order substructures of the 2D PCs with wider absolute gaps reported formerly are all optimal [10, 13].

In summary, our three-order-effect method may be useful for the designing of 2D PCs with larger absolute gaps.

ACKNOWLEDGMENT

This work was supported by the National Natural Science Foundation of China, Grant No. 10974061 and the Program for Innovative Research Team of the Higher Education in Guangdong, Grant No. 06CXTD005.

REFERENCES

1. Yablonovitch, E., "Inhibited spontaneous emission in solid-state physics and electronics," *Phys. Rev. Lett.*, Vol. 58, No. 20, 2059–2062, 1987.
2. John, S., "Strong localization of photons in certain disordered dielectric superlattices," *Phys. Rev. Lett.*, Vol. 58, No. 23, 2486–2489, 1987.
3. Jensen, J. S. and O. Sigmund, "Systematic design of photonic crystal structures using topology optimization: Low-loss waveguide bends," *Appl. Phys. Lett.*, Vol. 84, No. 12, 2022–2024, 2004.
4. Bjarklev, A., J. B. Jensen, J. Riishede, J. Broeng, J. Laegsgaard, T. Tanggaard Larsen, T. Sorensen, K. Hougaard, and O. Bang, "Photonic crystal structures in sensing technology," *Proc. of SPIE*, Vol. 5502, 9–16, 2004.
5. Maka, T., D. N. Chigrin, S. G. Romanov, and C. M. Sotomayor Torres, "Three dimensional photonic crystals in the visible regime," *Progress In Electromagnetics Research*, Vol. 41, 307–335, 2003.
6. Srivastava, R., S. Srivastava, and S. P. Ojha, "Negative refraction

- by photonic crystal,” *Progress In Electromagnetics Research B*, Vol. 2, 15–26, 2008.
7. Wu, J. J., D. Chen, K. L. Liao, T. J. Yang, and W. L. Ouyang. “The optical properties of Bragg fiber with a fiber core of 2-dimensional elliptical-hole photonic crystal structure,” *Progress In Electromagnetics Research Letters*, Vol. 10, 87–95, 2009.
 8. Qi, L. M., Z. Q. Yang, X. Gao, W. X. Liu, and Z. Liang, “Research on three types of rhombus lattice photonic band structures,” *Journal of Electromagnetic Waves and Applications*, Vol. 22, No. 8–9, 1115–1164, 2008.
 9. Ozbay, E., B. Temelkuran, and M. Bayindir, “Microwave applications of photonic crystals,” *Progress In Electromagnetics Research*, Vol. 41, 185–209, 2003.
 10. Anderson, C. M. and K. P. Giapis, “Larger two-dimensional photonic band gaps,” *Phys. Rev. Lett.*, Vol. 77, No. 14, 2949–2952, 1996.
 11. Kee, C. S., J. E. Kim, and H. Y. Park, “Absolute photonic band gap in a two-dimensional square lattice of square dielectric rods in air,” *Phys. Rev. E*, Vol. 56, No. 6, R6291–R6293, 1997.
 12. Shen, L. F., S. L. He, and S. S. Xiao, “Large absolute band gaps in two-dimensional photonic crystals formed by large dielectric pixels,” *Phys. Rev. B*, Vol. 66, No. 16, 165315-1–165315-6, 2002.
 13. Chern, R. L., C. C. Chang, C. C. Chang, and R. R. Hwang, “Large full band gaps for photonic crystals in two dimensions computed by an inverse method with multigrid acceleration,” *Phys. Rev. E*, Vol. 68, No. 2, 026704-1–026704-5, 2003.
 14. Anderson, C. M. and K. P. Giapis, “Symmetry reduction in group 4 mm photonic crystals,” *Phys. Rev. B*, Vol. 56, No. 12, 7313–7320, 1997.
 15. Malkova, N., S. Kim, T. Dilazaro, and V. Gopalan, “Symmetrical analysis of complex two-dimensional hexagonal photonic crystals,” *Phys. Rev. B*, Vol. 67, No. 12, 125203-1–125203-9, 2003.
 16. Zaccaria, R. P., P. Verma, S. Kawaguchi, S. Shoji, and S. Kawata, “Manipulating full photonic band gap in two dimensional birefringent photonic crystals,” *Opt. Express*, Vol. 16, No. 19, 14812–14820, 2008.
 17. Sigmund, O. and K. Hougaard, “Geometric properties of optimal photonic crystals,” *Phys. Rev. Lett.*, Vol. 100, No. 15, 153904-1–153904-4, 2008.